Numerical Study of Turbulent Liquid-Liquid Dispersions

Alexandra E. Komrakova
Chemical and Materials Engineering, University of Alberta, Edmonton, Alberta T6G 2V4, Canada

Dmitry Eskin
Schlumberger DBR Technology Center, Edmonton, Alberta T6N 1M9, Canada

J. J. Derksen
Chemical and Materials Engineering, University of Alberta, Edmonton, Alberta T6G 2V4, Canada

School of Engineering, University of Aberdeen, Aberdeen AB24 3UE, Scotland, U.K

DOI 10.1002/aic.14821
Published online April 20, 2015 in Wiley Online Library (wileyonlinelibrary.com)

A numerical approach is developed to gain fundamental insight in liquid-liquid dispersion formation under well-controlled turbulent conditions. The approach is based on a free energy lattice Boltzmann equation method, and relies on detailed resolution of the interaction of the dispersed and continuous phase at the microscopic level, including drop breakup and coalescence. The capability of the numerical technique to perform direct numerical simulations of turbulently agitated liquid-liquid dispersions is assessed. Three-dimensional simulations are carried out in fully periodic cubic domains with grids of size 100^3 to 1000^3. The liquids are of equal density. Viscosity ratios (dispersed phase over continuous phase) are in the range 0.3–1.0. The dispersed phase volume fraction varies from 0.001 to 0.2. The process of dispersion formation is followed and visualized. The size of each drop in the dispersion is measured in-line with no disturbance of the flow. However, the numerical method is plagued by numerical dissolution of drops that are smaller than 10 times the lattice spacing. It is shown that to mitigate this effect it is necessary to increase the resolution of the Kolmogorov scales, such as to have a minimum drop size in the range 20–30 lattice units [lu]. Four levels of Kolmogorov length scale resolution have been considered $\eta_K = 1$, 2.5, 5, and 10 [lu]. In addition, the numerical dissolution reduces if the concentration of the dispersed phase is increased.
AIChE J, 61: 2618–2633, 2015
Keywords: liquid-liquid, mixing, multiphase flow, turbulence, free energy lattice Boltzmann

Introduction

Turbulent agitation of two immiscible liquids to produce a liquid-liquid dispersion or emulsion is a common operation in chemical, petroleum, pharmaceutical, mining, and food industries. The dispersion is primarily formed as a result of drop interactions with turbulent eddies leading to drop breakup. Turbulent eddies with a size comparable to the drop size are efficient in disintegration of the dispersed phase. Smaller eddies only deform the drops, while larger eddies convect the drops with minor deformations. The evolution of eddy size and energy transformation in turbulent flow can be described by the Kolmogorov theory[1] which states that energy enters the system at the largest scales of motion. This energy is then transferred to successively smaller and smaller eddies with no dissipation until it is finally dissipated at the smallest (Kolmogorov) scales due to viscous effects. The energy cascade can be divided in two subranges: the inertial subrange where motions are determined by inertial effects and viscous effects are small, and a viscous subrange where effects of viscosity are dominant and energy is being dissipated. The behavior of the energy cascade in the inertial subrange is well described by the universal scaling law[1] $E(k) \sim \varepsilon^{2/3}k^{-5/3}$, where ε is the energy dissipation rate and k is the wavenumber. Many experimental studies on liquid-liquid dispersions have been performed in this subrange with drop sizes larger than the Kolmogorov scale.[2–8] As a result, numerous empirical and semiempirical correlations have been developed to predict the characteristic size of the drop, for example, the Sauter mean diameter or the maximum stable drop diameter (see Ref. 9 for a review of the correlations). On the other hand, the behavior of the two-phase turbulent system in the viscosity-dominated subrange is not well studied yet. Recent experimental work on liquid-liquid systems in this energy subrange has been performed by Boxall et al.[10] and Rueger and Calabrese.[11,12] Through rapid development of computational facilities, modelling and numerical simulation became valuable additions to experiment in order to study dispersed systems. A goal of this work is to develop a numerical approach to study turbulently flowing liquid-liquid dispersions both in inertial and viscous subrange.

This requires a two-phase flow method that resolves the interface. Interface-tracking (e.g., boundary-integral,[13] front tracking,[14] and immersed boundary[15]) and interface-

Correspondence concerning this article should be addressed to A. E. Komrakova at komrakov@ualberta.ca

capturing (level-set,[16] volume-of-fluid (VOF),[17] and coupled level-set VOF[18]) methods have been used to perform multiphase simulations. Interface-tracking methods use a separate grid to explicitly follow the interface motion. These methods are very accurate for simulating the onset of breakup and coalescence, but do not work through the transitions: in order to break or merge drops, complex somewhat arbitrary "cut-and-connect" algorithms have to be employed to change the topology of the meshes.[19] In interface-capturing methods, the interface is implicitly captured by scalar functions that use the data from the same fixed grid on which the flow is calculated. These methods do not require any "cut-and-connect" operations and automatically handle changes in interfacial topology which makes them suitable for simulating breakup and coalescence in immiscible two-fluid systems. The captured interface can be sharp or diffuse. In diffuse interface methods, the interface has finite thickness, and fluid properties change smoothly over the interface between two fluids. In this study, a diffuse interface free energy lattice Boltzmann equation (LBE) method[20] is adopted for turbulent liquid-liquid dispersion simulations. In this method, the physics of drop interaction on the microscopic level can be naturally incorporated. Moreover, the important advantages of LBE are simplicity of programming and parallelization of the algorithm which allows for very detailed simulations. On the other side, the interface between the liquids is significantly thicker than the physical interface. High resolution simulations are required to approach physically realistic interface thicknesses. As for the turbulent fluid flow simulations, it should be noted that three-dimensional decaying isotropic turbulence using lattice Boltzmann method was studied by Peng et al.[21] The authors rigorously compared their results to the results obtained from a pseudo-spectral method, and concluded that the LBE method is a reliable and accurate method for the direct numerical simulations (DNSs) of decaying turbulence.

To the best of author's knowledge, there is a lack of published data on numerical simulations of liquid-liquid flow in fully developed turbulence with resolution of drop/drop and drop/eddy interactions. The first attempt to perform DNSs of turbulent dispersed liquid-liquid flows using LBE has been done by Derksen and Van den Akker.[22] An isothermal model based on kinetic theory proposed by He et al.[23] was used for two-phase flow modeling. The authors presented a novel multiscale approach to model the dynamics of a liquid-liquid dispersion in a fully periodic three-dimensional domain in which homogeneous isotropic turbulence was generated by means of random forcing. The promising results showed that the numerical approach can contribute to understanding of turbulent agitation of immiscible liquids.

Droplet breakup in homogeneous and isotropic turbulence was numerically simulated by Toschi et al.[24] using LBE. The authors utilized the multicomponent Shan-Chen model[25] for two-phase flow modeling, supplemented with a large scale force to stir turbulence. The method was validated and applied for the study of turbulent emulsion flow[26]; the probability distribution function of droplets' accelerations was presented.

The droplet size distribution of water-in-oil type emulsions of a moderate viscosity ratio of 0.3 and with oil-soluble amphiphilic surfactant in forced, steady, homogeneous turbulence was studied using lattice Boltzmann simulations by Skartlien et al.[27] The details of the numerical method can be found in Ref. 28. The authors studied the effect of surfactant on the DSD defined under different levels of turbulent kinetic energy.

Baraldi et al.[29] has recently presented the results of DNSs of droplet-laden incompressible decaying isotropic turbulence in a simulation domain of 1024^3 where 7000 drops were initially injected. However, change of the drop size distribution (DSD) as a function of time and handling of the drop/drop interactions were not reported.

In this study, DNSs are performed to investigate a turbulently agitated liquid-liquid dispersion. The parallel computations are carried out in three-dimensional, fully periodic cubic domains. In such domain, stationary homogeneous isotropic turbulence is generated by means of linear forcing.[30] The domain edge L_d varied from 100 to 1000 dimensionless lattice units [lu].

The free energy LBE method for two-phase flow modeling is a diffuse interface method. In context of this method, the interface evolves naturally due to the thermodynamics employed. This issue gives a significant computational advantage over methods that require additional treatment of the interface. However, there is a drawback of the method which is dissolution of small droplets. As discussed by Keestra et al.[31] instead of bifurcating into two phases, small components remain a single phase at equilibrium. It is important to note that dissolution is not a mass conservation error. Through the course of the simulations mass and order parameter (introduced below) are conserved. The small drop dissolution is inherent property of the numerical method, not a numerical artifact. The rate of dissolution increases as the size of the drop decreases. Therefore, in order to mitigate the drop dissolution effect, it is necessary to increase the resolution of the Kolmogorov scales which are the smallest dynamic scales in the turbulent field, and generate the smallest size of drops in the range 20–30 [lu]. One of the goals of this study is to show that the dissolution effect can be mitigated if this condition is satisfied. The resolved Kolmogorov scales range from $\eta_K = 1$–10 [lu]. In addition, a drawback of the method is that it exhibits unphysically easy coalescence when drops are in close proximity.[32] This issue will also be addressed in this study.

The numerical method was verified and validated using simulations of drop deformation and breakup in simple shear flow.[33,34] The effects of interface-related numerical parameters on accuracy and stability were demonstrated by Komrakova et al.[33] The authors established guidelines on how to specify these parameters to reveal physically realistic drop behavior. These guidelines were successfully applied to investigate the effect of dispersed phase viscosity on the behavior of a sheared drop at a drop Reynolds number $Re = 10$ over a range of viscosity ratios $\lambda = 0.1-2$ (dispersed phase viscosity over continuous phase viscosity). The guidelines and results obtained in the sheared drop simulations of Komrakova et al.[33,34] are used in this study to determine the numerical parameters for turbulently flowing two-phase system. Effects of Kolmogorov scale resolution and dispersed phase volume fraction (ranging from 0.001 to 0.2) on dispersion formation are examined. The process of dispersion formation is visualized, capturing drop breakup, and coalescence on the microscopic scale. In each case, the DSD and mean diameters are determined and related to turbulent properties.

The physical size of a simulation domain is of the order of millimeters which is much smaller than the volume of any standard mixing device. However, the results obtained even in such a small domain can be useful for industrial

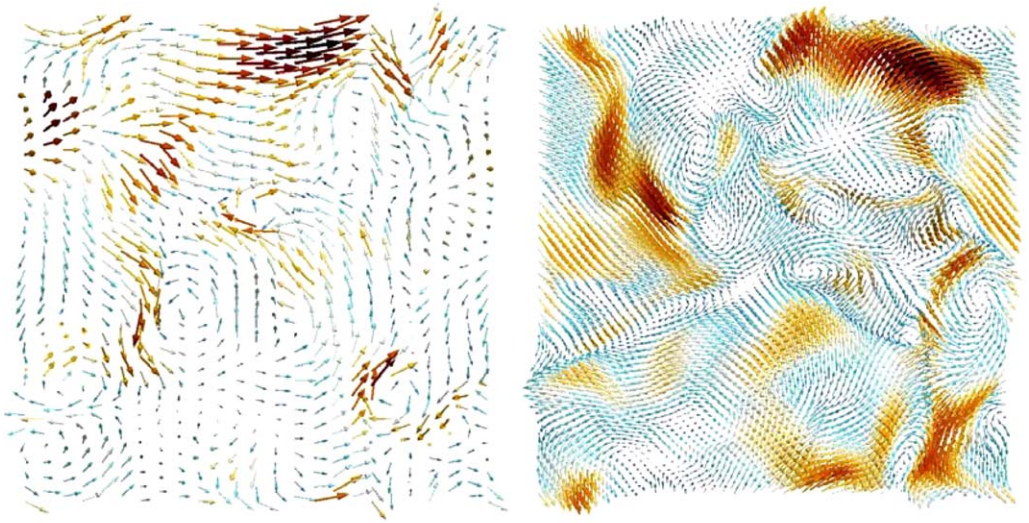

(a) (b)

Figure 1. Velocity vector fields of fully developed turbulent flow in the cross-sections of simulation domain.

(a) $\eta_K = 1$ [lu], $L_d = 100$ [lu]; (b) $\eta_K = 5$ [lu], $L_d = 500$ [lu]. Energy dissipation rate is the same in both cases. [Color figure can be viewed in the online issue, which is available at wileyonlinelibrary.com.]

applications by viewing it as a representative volume in a device as used in practice. A wide variety of mixing devices is used to produce liquid-liquid dispersions. Among them are stirred tanks, static mixers, and rotor-stator mixers. Each device has different geometry and capacity, creates various flow structures, and provides a range of agitation rates. The properties of the produced dispersion, such as stability, apparent viscosity, rheology, and interfacial area available for transfer processes, are determined by the size of the drops in the system. The DSD and the specific energy input (that is determined by the capabilities of a mixing device) are closely related.[11] It was experimentally demonstrated by Cutter[35] that in stirred tanks which are widely used for dispersion formation, the dissipation of power is inhomogeneous, which causes spatial variations of the DSD. Thus, the drop sizes can be related not to an average power input but to a local value of energy dissipation. Davies[6] showed that the relationship between the local power dissipation per unit mass of the liquid and the DSD (represented by the maximum stable drop diameter, d_{max}) is independent of the specifics of the mixer geometry, and can be applied for different mixing devices. Later Zhou and Kresta[36] experimentally proved an idea of Hinze[37] that the maximum local energy dissipation rate creates the stresses that eventually break the drops. Therefore, in order to break a drop to a desired size a certain intensity of the maximum local shear stress is needed which requires a specified local energy dissipation rate.[11] Thus, energy input per unit mass (or energy dissipation rate) in a domain in this study can be considered as a local value at some location in industrial equipment. Homogeneous isotropic turbulence generated throughout the domain minimizes the effects of nonhomogeneity, allowing to obtain fundamental results that can be used to perform scale-up.

Mathematical Formulation

Multiphase flow

A diffuse interface free energy LBE method proposed by Swift et al.[20] is adopted. In diffuse interface methods,[38–40] the interface is a transition region with a finite thickness where physical quantities vary continuously. The composition of the system is described by the order parameter φ which is the relative concentration of the two components.[41–43] The behavior of a binary mixture is simulated by solution of the continuity and momentum equations in conjunction with a Cahn-Hilliard convection-diffusion equation for the order parameter.[44] The evolution of density, velocity, and order parameter are governed by the continuity, momentum, and convection-diffusion equations, respectively[45]

$$\partial_t \rho + \partial_\alpha(\rho u_\alpha) = 0 \tag{1a}$$

$$\partial_t(\rho u_\alpha) + \partial_\beta(\rho u_\alpha u_\beta) = -\partial_\beta P^{th}_{\alpha\beta} + \partial_\beta \nu(\rho\partial_\alpha u_\beta + \rho\partial_\beta u_\alpha) + \rho F_{t\alpha} \tag{1b}$$

$$\partial_t \varphi + \partial_\alpha(\varphi u_\alpha) = M\partial^2_{\beta\beta}\mu \tag{1c}$$

where u_α is the velocity; the index α stands for the Cartesian directions x, y, and z; ρ and ν are the density and the kinematic viscosity of the mixture, respectively; M is the mobility; $F_{t\alpha}$ is the forcing term to generate turbulence (discussed below). Here $P^{th}_{\alpha\beta}$ is the "thermodynamic" pressure tensor. It contains two parts[45]: an isotropic contribution $P\delta_{\alpha\beta}$ that represents the ideal gas pressure and the "chemical" pressure tensor $P^{chem}_{\alpha\beta}$. As $P^{chem}_{\alpha\beta}$ is a function of order parameter φ, the latter one is an active scalar and the set of Eq. 1 is intimately coupled. The chemical potential in Eq. 1c is: $\mu(\varphi) = A\varphi - A\varphi^3 - \kappa\partial^2_{\alpha\alpha}\varphi$. Here, $A < 0$ and κ are parameters of the free energy model that are related to the surface tension and interface thickness.

Two distribution functions are utilized to solve system (1): one function $f(\boldsymbol{r}, t)$ is used to solve the continuity (1a) and Navier-Stokes (1b) equations and the second one $g(\boldsymbol{r}, t)$ is used for the convection-diffusion Eq. 1c. The distribution functions evolve by a time step Δt. All simulations have been performed using a single relaxation time collision operator (Bhatnagar-Gross-Krook model[46]). The discrete LBEs for the evolution of f and g have the following form

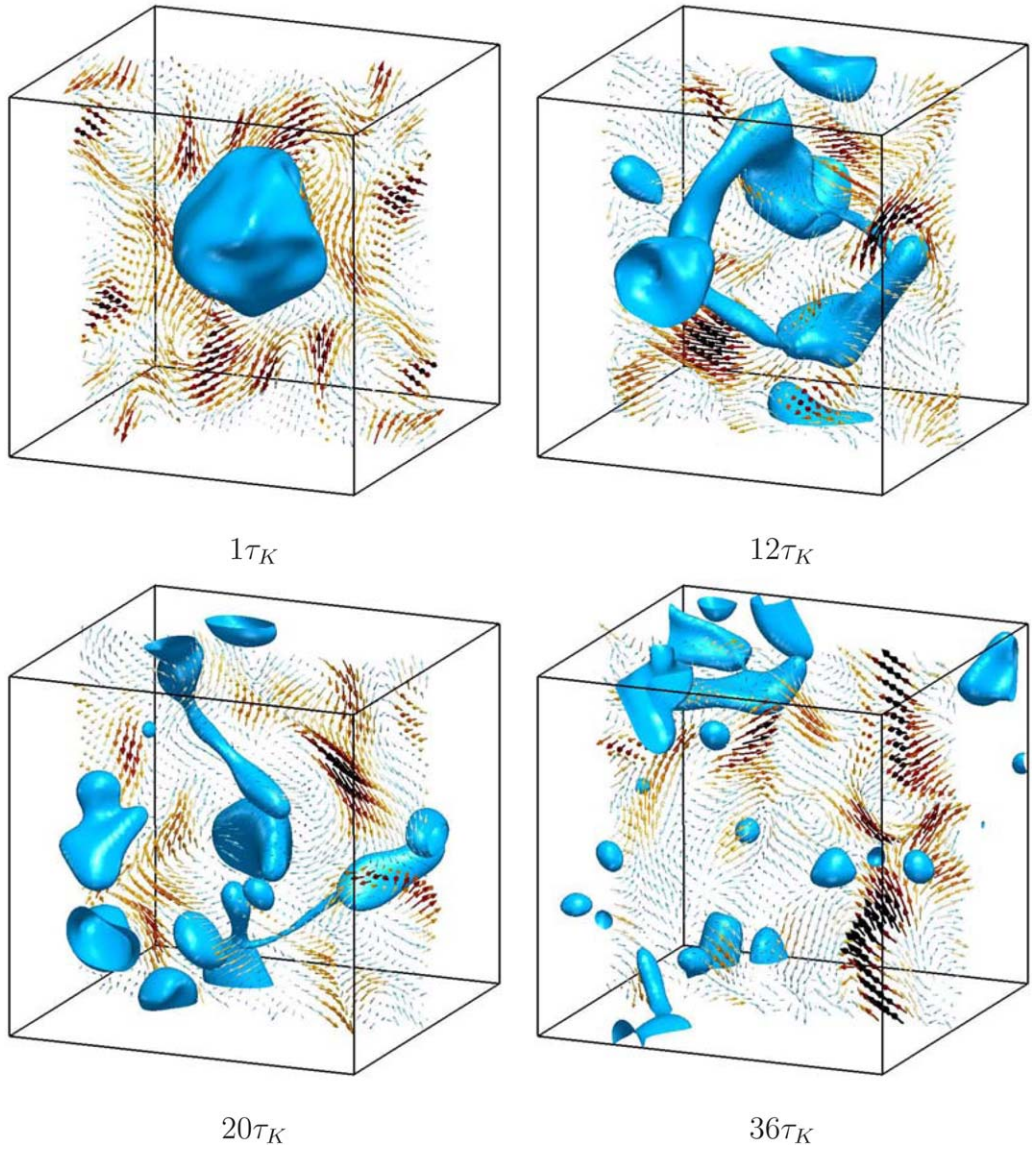

Figure 2. Iso-surfaces of order parameter $\varphi = 0$ and velocity fields at different time instants relative to the Kolmogorov time scale τ_K for the case with $\eta_K = 1$ [lu], viscosity ratio $\lambda = 1$ and the capillary number $Ca = 0.1$.

The dispersed phase volume fraction is $\phi = 0.03$. The moment of drop injection is $t = 0$. [Color figure can be viewed in the online issue, which is available at wileyonlinelibrary.com.]

$$f_q(r_\alpha + c_{\alpha q}\Delta t, t+\Delta t) - f_q(r_\alpha, t) = -\frac{f_q - f_q^{\mathrm{eq}}}{\tau_f} + F_q, \qquad (2a)$$

$$g_q(r_\alpha + c_{\alpha q}\Delta t, t+\Delta t) - g_q(r_\alpha, t) = -\frac{g_q - g_q^{\mathrm{eq}}}{\tau_g}, \qquad (2b)$$

where the index q counts over the number of the discrete velocity directions; f_q^{eq}, g_q^{eq} are the discretized Maxwell-Boltzmann distributions (or equilibrium distributions); F_q is the forcing term; $c_{\alpha q}$ denotes the discrete velocity set and τ_f and τ_g are dimensionless relaxation parameters. The equilibrium distributions f_q^{eq}, g_q^{eq} are given in Kusumaatmaja.[47] The D3Q19 lattice is adopted here where $D = 3$ denotes three-dimensional flow and $Q = 19$ is the number of velocities including a zero velocity. In this lattice arrangement, each site communicates with its six nearest and twelve diagonal neighbors. The lattice Boltzmann method operates in dimensionless lattice units [lu] (lattice space, time step, and lattice density for the length, time and mass units, respectively). For the method described here, only uniform cubic lattices can be used; the mesh step Δx is taken as unity, as is the time step Δt.

The distribution functions are defined such that the following summations over all directions q at each lattice point give the local density of the fluid ρ, the local fluid momentum ρu_α and the local order parameter φ, respectively

$$\sum_q f_q = \rho \qquad \sum_q c_{\alpha q} f_q = \rho u_\alpha + \frac{F_{t\alpha}}{2} \qquad \sum_q g_q = \varphi \qquad (3)$$

The forcing term (Eq. 2a) is incorporated as follows

$$F_q = w_q(c_{\alpha q} F_{t\alpha}) \qquad (4)$$

where $F_{t\alpha}$ is the macroscopic force embedded in momentum Eq. 1b and w_q are weight coefficients.[47]

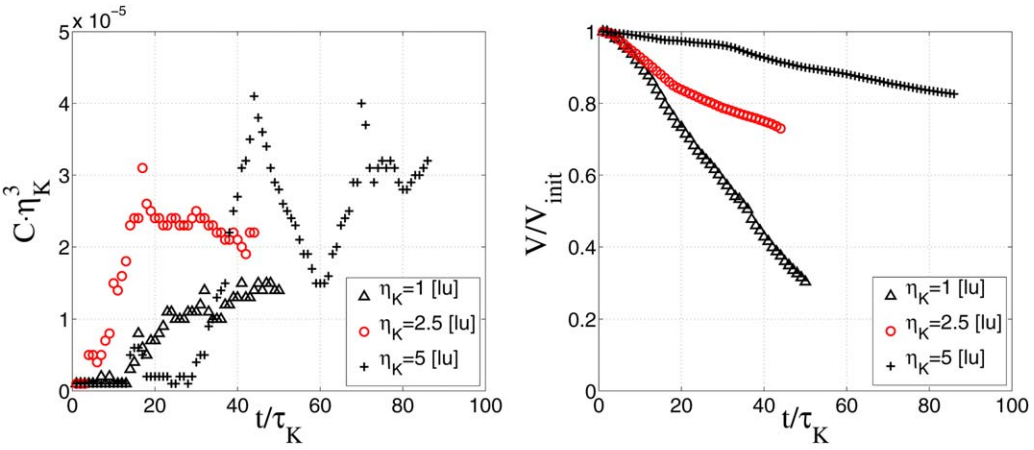

(a) (b)

Figure 3. Number concentration *C* (a) and dispersed volume *V* in the system relative to the initial value V_{init} (b) as functions of time for the cases with different Kolmogorov length scale resolution.

Viscosity ratio is $\lambda = 1$, the capillary number is $Ca = 0.1$, the dispersed phase volume fraction is $\phi = 0.03$ [Color figure can be viewed in the online issue, which is available at wileyonlinelibrary.com.]

In order to consider two liquids with different kinematic viscosities, the kinematic viscosity of the mixture v is set to be a linear function of the order parameter φ

$$v(\varphi) = v_c \frac{\varphi_0 - \varphi}{2\varphi_0} + v_d \frac{\varphi_0 + \varphi}{2\varphi_0} \tag{5}$$

where v_c and v_d are the kinematic viscosities of continuous and dispersed phases, respectively; and $\varphi = \pm\varphi_0 = \pm 1$ is the value of the order parameter in the bulk phase on either side of the interface. The relaxation parameter for f_q varies with the composition[20] as follows

$$\tau_f(\varphi) = \frac{v(\varphi)}{c_s^2} + \frac{1}{2} \tag{6}$$

Here, $c_s^2 = 1/3$ is the speed of sound in lattice units. The mobility M (see Eq. 1c) is determined by the coefficient of mobility Γ and the relaxation parameter τ_g according to relation[20]

$$M = \Gamma\left(\tau_g - \frac{1}{2}\right) \tag{7}$$

For a planar interface, an analytical solution[48] gives the φ profile $\varphi(x) = \varphi_0 \tanh(x/\xi)$ (x is the coordinate normal to the interface). The thickness of the diffuse interface is characterized by the characteristic length ξ

$$\xi = \left(\frac{2\kappa}{-A}\right)^{1/2}. \tag{8}$$

The interfacial tension σ follows from

$$\sigma = \frac{4}{3}\kappa\frac{\varphi_0^2}{\xi}. \tag{9}$$

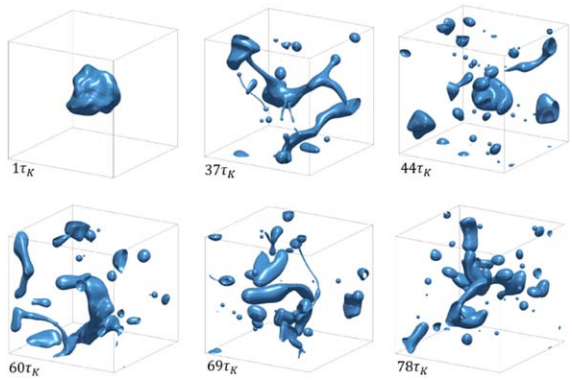

Figure 4. Iso-surfaces of order parameter $\varphi = 0$ at different time instants relative to the Kolmogorov time scale τ_K for the case with $\eta_K = 5$ [lu].

The viscosity ratio is $\lambda = 1$, the capillary number is $Ca = 0.1$ and the dispersed phase volume fraction is $\phi = 0.03$. The moment of drop injection is $t = 0$. [Color figure can be viewed in the online issue, which is available at wileyonlinelibrary.com.]

Turbulence generation

Statistically stationary homogeneous isotropic turbulence is generated throughout the simulation domain. The viscous dissipation extracts energy from the system. To sustain a constant turbulence during the simulation, the energy input is organized by means of forcing. The linear forcing proposed by Lundgren[30] is adopted here. A local force proportional to the local velocity is imposed on the liquid. In this case, the momentum Eq. 1b gets a forcing term $F_{t\alpha} = A_f u_\alpha$ and the parameter A_f is determined as

$$A_f = \frac{\varepsilon}{3u_{rms}^2} \tag{10}$$

where ε is the volume-averaged energy dissipation rate per unit mass which is an input parameter, and u_{rms} is the volume-averaged root-mean-square fluid velocity which is an output parameter calculated every time step.

A detailed exploration of linear forcing has been carried out by Rosales and Meneveau.[49] These authors confirmed that the linear force implementation in physical space gives the same results as when applied in spectral space. However, they pointed out that with linear forcing the integral length

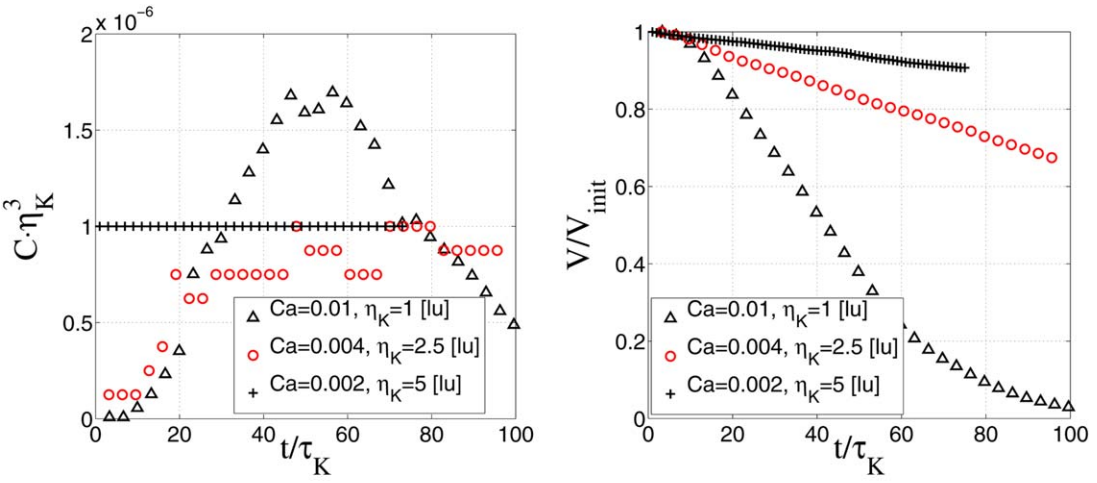

(a) (b)

Figure 5. Number concentration *C* (a) and dispersed volume *V* in the system relative to the initial value V_{init} (b) as functions of time for the case with different energy input and the Kolmogorov length scale resolution η_K.

The viscosity ratio is $\lambda = 1$, the dispersed phase volume fraction is $\phi = 0.005$. [Color figure can be viewed in the online issue, which is available at wileyonlinelibrary.com.]

scale is a smaller fraction of the domain size than with band-limited forcing. As a result, to achieve a given Reynolds number higher resolution for linear forcing is required than for spectral forcing. Also in order to achieve statistical stationary quantities, it is necessary to run simulations for longer period of time. In this study, several levels of resolution of the smallest (Kolmogorov) scales have been explored in a large scale domain. To generate fully-developed single-phase turbulence every simulations has been conducted long enough to ensure time-invariant statistics before introducing dispersed phase. In addition, this type of forcing was successfully implemented in the context of the LBE method by several authors,[50,51] including applications in multiphase flow.

The turbulence generation method requires a non-zero velocity field to start with. Thus, at $t = 0$ the velocity field was initialized using the following relations[50]

$$u_x = u_{\text{init}} \sin\left(\frac{2\pi j}{\lambda_0}\right) \quad u_y = u_{\text{init}} \sin\left(\frac{2\pi k}{\lambda_0}\right) \quad u_z = u_{\text{init}} \sin\left(\frac{2\pi i}{\lambda_0}\right) \tag{11}$$

where $\lambda_0 = 1.01L_d/4$, $i = j = k = (1 : L_d)$ (corresponding to x, y, and z, respectively); $u_{\text{init}} = 5u_K$ is the maximum velocity in the initial distribution; L_d is the domain edge size; and u_K is the Kolmogorov velocity scale. This flow field is divergence free.

The resolution of the Kolmogorov scales varied in the simulations. As an example, the velocity magnitude fields in the cross-sections of the domain when the turbulence is fully developed for $\eta_K = 1$ and 5 [lu] are presented in Figure 1. In both cases energy input (or energy dissipation rate ε) is the same and the separation of scales which is a ratio of simulation domain edge to the Kolmogorov length scale L_d/η_K is 100.

Simulation Parameters

The binary liquid system agitated by linear forcing can be described by the following set of input parameters (subscripts d and c refer to the dispersed and continuous phases, respectively): the kinematic viscosities of liquids ν_d, ν_c, the densities of liquids ρ_d, ρ_c, the interfacial tension σ, the energy dissipation rate ε, the dispersed phase volume V_d and the total volume of liquids V_t. Taking into account that only liquids of equal densities are considered here $\rho_d = \rho_c = \rho$, the set of parameters can be reduced to three independent dimensionless numbers which are a capillary number $Ca = \dot{\gamma} l \nu_c \rho/\sigma$, a viscosity ratio $\lambda = \mu_d/\mu_c$ and dispersed phase volume fraction $\phi = V_d/V_t$. Here, $\dot{\gamma}$ is the characteristic shear rate, and l is the characteristic length scale. The length and time scales can be estimated based on the corresponding Kolmogorov scales: $l = \eta_K = (\nu_c^3/\varepsilon)^{1/4}$ and $\dot{\gamma} = 1/\tau_K = (\varepsilon/\nu_c)^{1/2}$. Then the capillary number is $Ca = \rho \nu_c^{5/4} \varepsilon^{1/2}/\sigma$. Note that Reynolds number defined using Kolmogorov scales is equal to unity.[1] An alternative option to characterize turbulent flow is by giving the Taylor-microscale Reynolds number defined as $Re_{\lambda_T} = u_{\text{rms}} \lambda_T/\nu$ where λ_T is the Taylor microscale[1] $\lambda_T = (15\nu u_{\text{rms}}^2/\varepsilon)^{0.5}$. However, Re_{λ_T} cannot be used as an input parameter since it contains the root-mean-square velocity u_{rms} which is an output parameter of the simulations. Thus, Ca, λ and ϕ fully determine the two-phase turbulent system.

In addition to physical dimensionless numbers, the numerical parameters should be specified. Lattice Boltzmann methods operate in lattice space, and, all parameters have been defined in lattice units. For the adopted LBE method, the density value in the incompressible limit is equal to unity. Thus, the density of continuous ρ_c and dispersed ρ_d phases in lattice space is set to $\rho_c = \rho_d = 1$ in lattice units [lu]. Since the liquids are of equal density, the dynamic and kinematic viscosities of the liquids are effectively the same. The kinematic viscosity of the continuous liquid is related to the relaxation time for the f_q distribution function as follows: $\nu_c = c_s^2(\tau_f - 0.5)$. The relaxation time corresponding to the continuous phase is set to 0.51 or 0.53 depending on the value of the energy input. These values are specified to satisfy the incompressibility limit, that is, the velocity fluctuations in lattice units should not be greater than $0.1c_s$

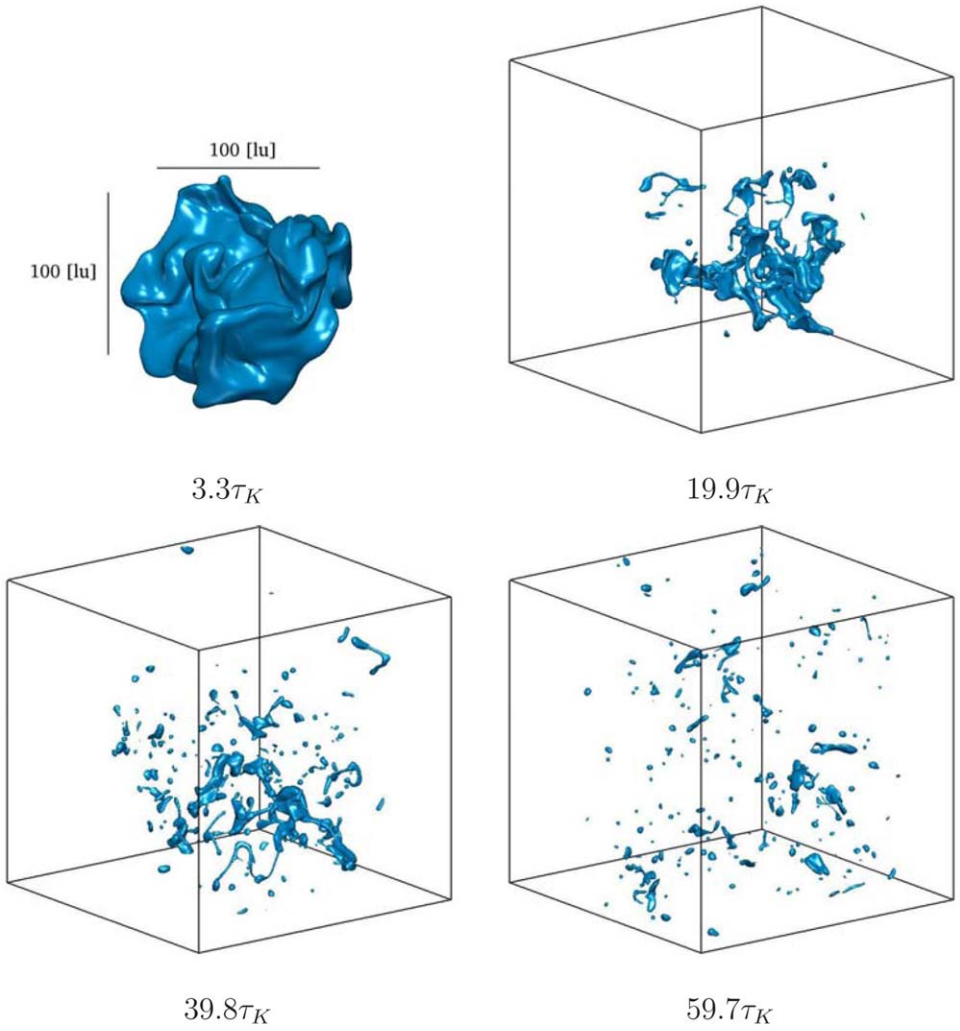

Figure 6. Isosurfaces of order parameter $\varphi = 0$ at different time instants relative to the Kolmogorov time scale τ_K for the case with $\eta_K = 1$ [lu], viscosity ratio $\lambda = 1$ and capillary number $Ca = 0.01$.

The dispersed phase volume fraction is $\phi = 0.005$. The moment of drop injection is $t = 0$. [Color figure can be viewed in the online issue, which is available at wileyonlinelibrary.com.]

(Ref. 52). The kinematic viscosity of the dispersed phase (and the related relaxation time) is determined based on the ratio of dispersed to continuous phase viscosities $\lambda = \mu_d/\mu_c$. The relaxation time for the second distribution function g_q is set to unity in each simulation: $\tau_g = 1$.

Special care should be taken when setting up the numerical parameters related to the interface, which are: the interface thickness ξ, the free energy model parameters A and κ, the mobility M, and the coefficient of mobility Γ. The optimal values of these parameters are related to the drop size[33] which varies during dispersion formation. Being exposed to continuously changing turbulent flow, drops undergo a variety of simultaneously occurring events caused by interactions with turbulent eddies that convect, deform, merge, and break them. However, a connection with the flow in a simpler geometry, such as simple shear flow, can help to optimize the interface-related numerical parameters. For example, a drop in a simple shear flow is akin to a drop interacting with two corotating eddies in turbulent flow. It was outlined by Komrakova et al.[33] that for a drop in simple shear flow numerical parameters related to the interface are determined by two dimensionless numbers: the interface Peclet number $Pe = \dot{\gamma} a \xi/(MA)$, that relates the convection time scale to the interface diffusion time scale, and the Cahn number $Ch = \xi/a$ that is the ratio of the interface thickness and drop radius. Here, $\dot{\gamma}$ is the shear rate, and a is the drop radius. It was shown that the accuracy of drop deformation and breakup simulations is determined by mesh resolution and can be adjusted by Pe and Ch. High-resolution drops with radii larger than 30 [lu] require a thicker interface $\xi \geq 2$ [lu], while drops with $a < 30$ [lu] need thinner interfaces.[33] The goal of the present simulations is to resolve small drops after multiple breakup processes. Therefore, the interface thickness is set to $\xi = 1.14$ [lu]. The values of A and κ are related to the interfacial tension (see Eqs. 8 and 9) which is set to $\sigma = 0.01$ [lu]. According to a guideline of Komrakova et al.[33] higher interfacial tension (or bigger κ) from a range that allow stable simulations requires a smaller diffusion coefficient Γ. Based on their range of κ and Γ values, the diffusion coefficient in the present simulations is set to $\Gamma = 4$. The rest of the parameters are $\kappa = 0.009$, $A = -0.014$, and $M = 2$.

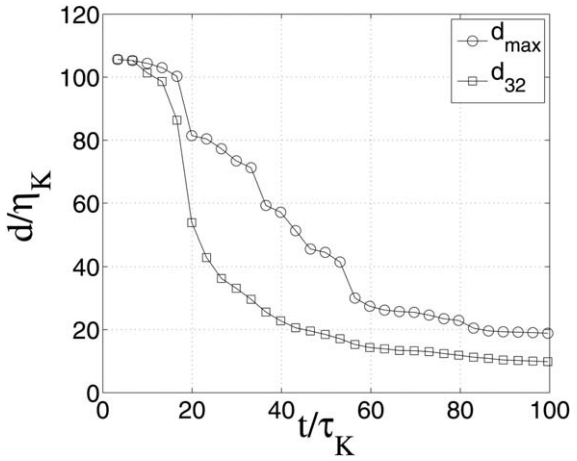

Figure 7. Dimensionless maximum d_{max} and Sauter mean d_{32} diameters as a function of time for the case with Kolmogorov length scale resolution $\eta_K = 1$ [lu], viscosity ratio $\lambda = 1$ and capillary number $Ca = 0.01$.

The dispersed phase volume fraction is $\phi = 0.005$.

Each simulation is performed in a fully periodic cubic domain with an edge length L_d. Cases with $L_d = 100$, 250, 500, and 1000 [lu] are examined. The simulations are carried out in the following way. Homogeneous isotropic turbulence with a given energy dissipation rate in a single phase is generated throughout the domain. Then the second phase is injected. The liquid-liquid interface is represented as isosurface with the order parameter $\varphi = 0$. Positive φ values represent the dispersed phase, negative φ values refer to the continuous phase. The transition region between -1 and 1 is the interface. A drop is identified as a connected volume with positive φ. The DSD of the steady state dispersion is characterized by two representative drop sizes: the Sauter mean diameter d_{32}, and the maximum stable drop diameter, d_{max}, that resists breakup. The Sauter mean diameter is the ratio of the third and the second moment of the DSD

$$d_{32} = \frac{\sum_{i=1}^{k} d_i^3}{\sum_{i=1}^{k} d_i^2} \tag{12}$$

where d_i is the diameter of drop i and k is the number of drops in the system. Drop sizes are expressed in terms of their volume-equivalent diameter $d_i = (6V/\pi)^{1/3}$. The d_{32} is directly related to the interfacial area per unit volume a_V in the dispersion which is an important industrial parameter: $d_{32} = 6\phi/a_V$ (where ϕ is the holdup of the dispersed phase).

The computer code was implemented in Fortran 90 with message passing interface for parallel processing. The fully periodic three-dimensional domain was divided into equal cubic subdomains in every direction, one for each CPU. Large-scale simulation with domain size of 500^3 and 1000^3 were performed using 125 CPUs. The processing time varied from two days for the simulation in a 500^3 domain and up to 2 months for continuous simulations in a 1000^3 domain depending on the resolution of the Kolmogorov scales: higher resolution of the Kolmogorov time scale requires larger number of time steps to simulate the same time interval as in the case with the lower resolution of τ_K.

Dispersion Formation

Effect of Kolmogorov scale resolution

In order to check the sensitivity of the results with respect to the Kolmogorov scale resolution, simulations with the following physical parameters have been performed: $Ca = 0.1$, $\lambda = 1$, $\phi = 0.03$. Three levels of Kolmogorov length scale resolution are considered $\eta_K = 1$, 2.5, and 5 [lu]. The smallest domain corresponding to $\eta_K = 1$ [lu] has the edge $L_d = 100$ that means the scale separation is $L_d/\eta_K = 100$. The L_d/η_K ratio remained constant with an increase of η_K resolution. In each case a single droplet was injected into the fully developed turbulent flow.

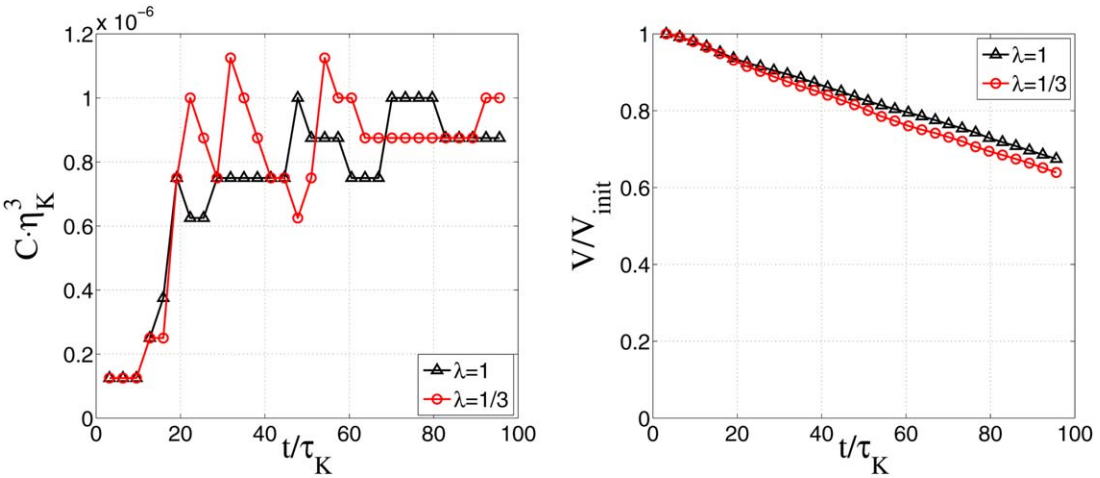

(a) (b)

Figure 8. Number concentration C (a) and dispersed volume V in the system relative to the initial value V_{init} (b) as functions of time for the cases with Kolmogorov length scale resolution $\eta_K = 2.5$ [lu], viscosity ratio $\lambda = 1$ and 1/3, capillary number $Ca = 0.004$.

The dispersed phase volume fraction is $\phi = 0.005$. [Color figure can be viewed in the online issue, which is available at wileyonlinelibrary.com.]

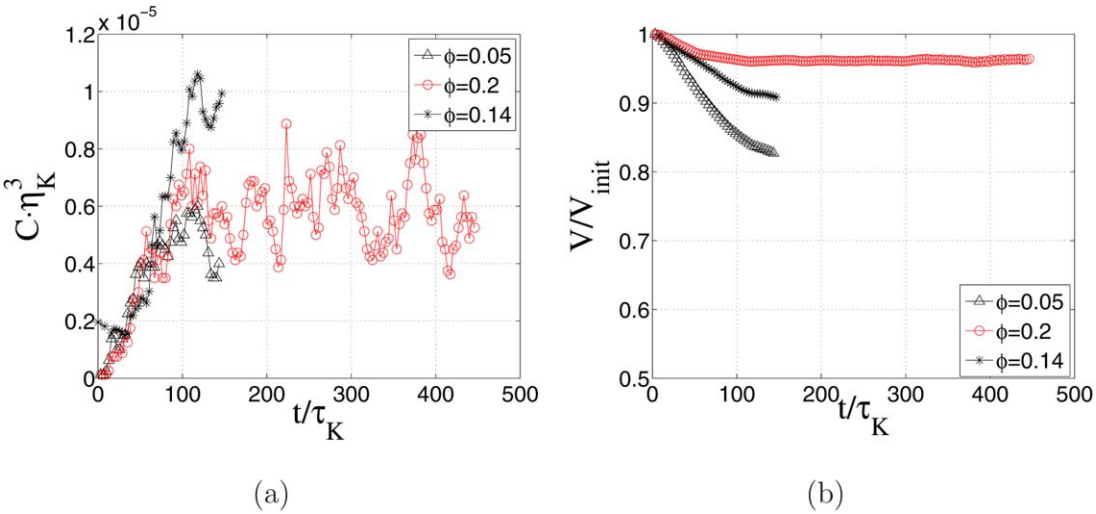

Figure 9. Number concentration *C* (a) and dispersed volume *V* in the system relative to the initial value V_{init} (b) as functions of time for the cases with different values of dispersed phase fraction.

The Kolmogorov length scale resolution is $\eta_K = 2.5$ [lu], the viscosity ratio is $\lambda = 1$, the capillary number is $Ca = 0.004$. [Color figure can be viewed in the online issue, which is available at wileyonlinelibrary.com.]

The dispersion formation process for the case with $\eta_K = 1$ [lu] is visualized by plotting the isosurfaces of the order parameter $\varphi = 0$ (which represents the liquid-liquid interface) at the different time instances (see Figure 2). The velocity fields in the cross-sections of the domain are also depicted. At the moment $t = 1\tau_K$ after the drop injection, the drop is deformed due to interactions with turbulent eddies which are smaller in size than the drop. By the time $t = 12\tau_K$, the drop is significantly deformed, but remains as a single structure. Thin threads are formed in a way as if the drop is exposed to shear flow. Finally, the drop is broken into smaller fragments (see $t = 36\tau_K$). It should be noted that in turbulent flow drops are mainly broken by end-pinching mechanism[53]: bulbs form at the ends of the stretched drop and pinch off. The drop can be significantly elongated before breakup which results in formation of a thin thread. This thread breaks into small fragments. However, the mechanism of the breakage is not obvious: it can be triggered by pressure fluctuations which lead to capillary wave breakup or it can still be end-pinching.

As the numerical method is plagued by numerical dissolution of small drops, satellite, and subsatellite drops disappear almost immediately after generation. Initially, the number of drops increases due to breakup, reaches a maximum, and then decreases to zero. A decrease in the number of drops can be explained by simultaneously occurring drop coalescence and dissolution events. The numerical dissolution is not a mass loss. In the present simulations mass and order parameter are conserved. The dissolution of small drops is an inherent mechanism of Cahn-Hilliard dynamics when dispersed and continuous phases instead of separation remain as a single phase at equilibrium.[31] There exists a critical drop size below which the drop dissolves. Thus, to reduce the dispersed phase dissolution, it is suggested to increase the resolution so that the minimum size of the drops after breakup is in the range 20 to 30 lattice units.

Simulations with higher resolution of Kolmogorov scales indeed resulted in mitigation of numerical dissolution of the drops. In order to compare different cases, the number of drops is represented by a number concentration C which is a ratio of number of drops to the simulation domain volume. The number concentration as a function of time with different η_K resolution is shown in Figure 3a and the ratio of the dispersed phase volume V to the initial drop volume V_{init} is plotted vs. time in Figure 3b. If $\eta_K = 1$ [lu] and $t = 50\tau_K$, 70% of the dispersed phase is dissolved which means the number of drops is underestimated compared to the system with no numerical dissolution. When $\eta_K = 5$ [lu], less than 20% of the dispersed phase is dissolved by $t = 80\tau_K$. The number of drops is changing due to breakup and coalescence events. However numerical dissolution of small drops should still be taken into account. It is necessary to note that due to significant dissolution, the stationarity for the cases shown in Figure 3 has not been reached during the specified simulation time.

The dispersion formation process when $\eta_K = 5$ [lu] is depicted in Figure 4. The initially spherical drop is deformed and ruptured by turbulent eddies. High-resolution allows observing formation and evolution of microscopic structures as thin threads, bulbs, satellites and subsatellites, and complex drop deformations. When the threads of the drop formed by the time instant $37\tau_K$ eventually break, multiple satellite and subsatellite drops are produced (see time instant $44\tau_K$ that corresponds to the maximum number of drops in the system). After this time due to joint effect of coalescence and numerical dissolution, the number of drops decreases ($t = 60\tau_K$). As a result of coalescence, larger drops appear. These drops are unstable and can be deformed by turbulent eddies ($t = 69\tau_K$) and broken into smaller fragments again ($t = 78\tau_K$).

Effect of energy input

Large-scale simulations with $L_d = 500$ [lu] for different energy input characterized by capillary number $Ca = 0.01$, 0.004, and 0.002 and 0.001 and varying resolution of the Kolmogorov length scale from 1 to 10 lattice units have been performed at the viscosity ratio $\lambda = 1$ and the dispersed phase volume fraction $\phi = 0.005$. The Reynolds number based on the Taylor microscale is equal to 141, 56, 40, and 24 for each case, respectively.

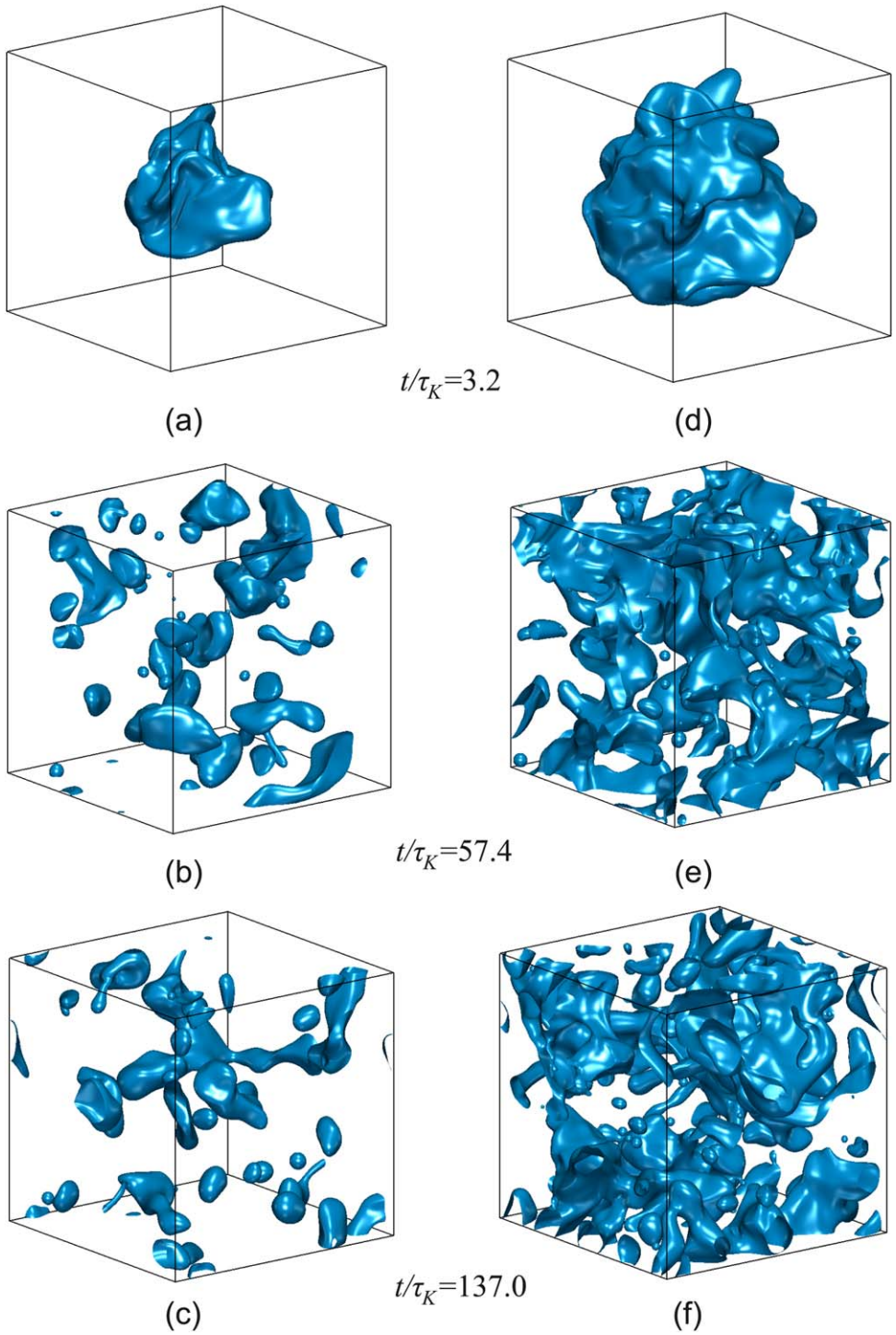

Figure 10. Isosurfaces of order parameter $\varphi = 0$ at different time instants relative to the Kolmogorov time scale τ_K for the case with $\eta_K = 2.5$ [lu]; (a)–(c) dispersed phase volume fraction is $\phi = 0.05$; (d)–(f) dispersed phase volume fraction is $\phi = 0.2$.

Viscosity ratio is $\lambda = 1$, capillary number $Ca = 0.004$. The moment of drop injection is $t = 0$. [Color figure can be viewed in the online issue, which is available at wileyonlinelibrary.com.]

The number concentration and dispersed phase volume as the functions of time are presented in Figures 5a and b, respectively. In each case, the simulation was stopped before the statistical stationarity is reached. For the cases with $Ca = 0.002$ and 0.001, the energy input was not enough to break the drop. If at $Ca = 0.002$, the drop was slightly deformed, at $Ca = 0.001$ the drop remained spherical for the entire simulation. For the latter case the dimensionless number concentration was 8×10^{-6}. As one can see from Figure 5b, the dispersed phase dissolution decreases with the increase of the Kolmogorov scale resolution. The decrease of energy input (and thus energy dissipation rate) leads to decrease of numerical dissolution.

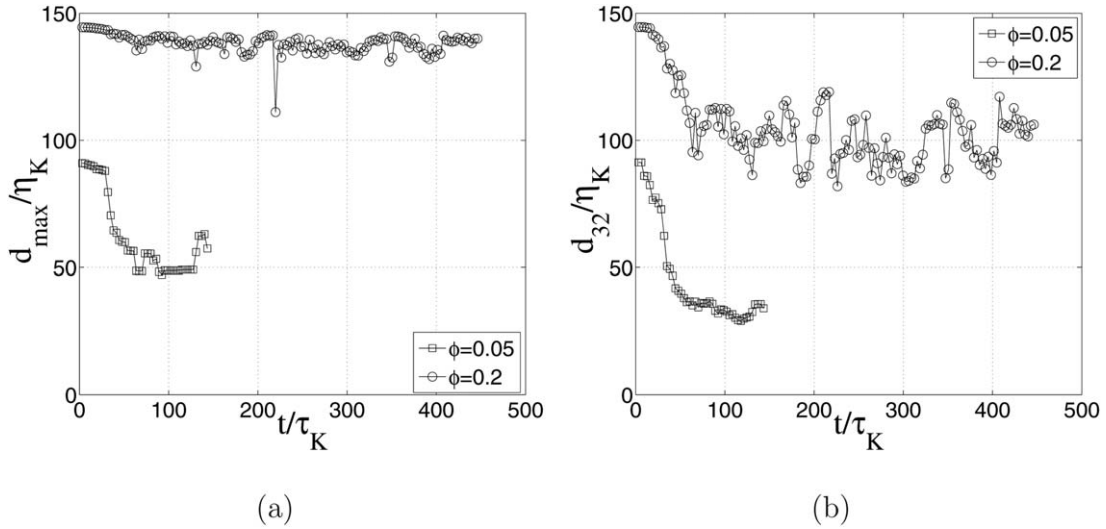

Figure 11. Dimensionless maximum d_{max} (a) and Sauter mean d_{32} (b) diameters as functions of time for the case with Kolmogorov length scale resolution $\eta_K = 2.5$ [lu], viscosity ratio $\lambda = 1$, capillary number $Ca = 0.004$.

The dispersed phase volume fraction is $\phi = 0.05$ and 0.2.

Consider the results of a simulation characterized by capillary number $Ca = 0.01$. A single droplet with initial undeformed diameter of $106\eta_K$ was injected into the fully developed turbulent flow. The dispersion formation process is visualized by plotting the isosurfaces of the order parameter $\varphi = 0$ at different time instances (Figure 6). At the moment $t = 3.3\tau_K$ starting from the drop injection, the drop is already significantly deformed. By the time $t = 19.9\tau_K$, small droplets have formed. The large dispersed phase structure is, however, not yet disintegrated. Finally, the drop is broken into small fragments (see $t = 59.7\tau_K$).

By the time $t = 59.7\tau_K$, most of the drops have diameters less than $10\eta_K$ ($d < 10$ [lu]) approaching the viscous subrange of the energy spectrum. When the drop size becomes comparable to the Kolmogorov length scale, the drops interact with the eddies that create shear of the order of $\dot{\gamma} = 1/\tau_K$. In order to compare this drop-flow interaction to a drop in simple shear flow, the dimensionless numbers based on drop radius a are used. The Reynolds number for a drop with radius $a = 5$ [lu] is $Re = \dot{\gamma}a^2/\nu_c = 25$. The drop capillary number is $Ca = a\dot{\gamma}\mu_c/\sigma = 0.05$. In order to break the drop, the critical capillary number Ca_c should be exceeded. According to the results presented by Khismatullin et al.,[54] who studied drop breakup in simple shear flow, the critical capillary number at $Re = 10$ is $Ca_c = 0.147$ and at $Re = 50$ is $Ca_c = 0.058$ for $\lambda = 1$. This means that at $Re = 25$ the critical capillary number is in between these two values. Consequently, the drops of radii $\sim$5 [lu] and smaller might not be broken under the present agitation conditions. However, complex interactions with multiple eddies might lead to drop breakup. Droplets of diameter $\sim\eta_K$ could be satellites and subsatellites formed after breakup of larger droplets. Figure 7 presents the maximum drop diameter and the Sauter mean diameter as functions of time. Because of dissolution both of them eventually approach zero.

Effect of viscosity ratio

The viscosity ratio influence λ has been tested on a case characterized by $Ca = 0.004$ and the resolution of the Kolmogorov length scale $\eta_K = 2.5$ [lu]. The simulations were performed in a 500^3 domain with one initial drop of diameter $d = 42.4\eta_K$ [lu] that results in a dispersed phase volume fraction $\phi = 0.005$. Two viscosity ratios were examined $\lambda = 1$ and 1/3. The number concentration as a function of time for $\lambda = 1$ and 1/3 is shown in Figure 8a. Due to high level of numerical dissolution, in each case the simulation was stopped before the statistical stationarity is reached.

The factor of three differences in viscosity between the liquids is not sufficient to see a prominent difference in the number of drops generated. When $\lambda = 1/3$, the internal viscous stresses that counteract stresses caused by pressure fluctuations become weaker. Therefore, more drops should form compared to the case with $\lambda = 1$. However generation of more satellite and subsatellite drops (that are small in size) leads to faster drop dissolution (see Figure 8b). As a result, number concentration almost does not change with the viscosity ratio (see Figure 8a).

Effect of dispersed phase volume fraction

Liquid-liquid dispersion formation at high loadings of dispersed phase was examined for the cases with the Kolmogorov length scale resolution $\eta_K = 2.5$ [lu], capillary number $Ca = 0.004$, equal phase viscosities, and at dispersed phase volume fractions $\phi = 0.05$ and 0.2. The simulations were carried out in a 500^3 domain. The initial size of the injected drop was $91.0\eta_K$ and $144.5\eta_K$ for $\phi = 0.05$ and 0.2, respectively. A simulation with $\eta_K = 2.5$ [lu], Ca = 0.004 and $\lambda = 1$ was also performed on a larger scale with domain edge size $L_d = 1000$ [lu]. As the initial condition, 125 drops of diameter $46.3\eta_K$ were injected into a fully developed turbulent flow. The dispersed phase volume fraction in this case is $\phi = 0.14$.

A higher dispersed phase volume fraction significantly reduces the dissolution. The dissolution results in an increase in the order parameter φ in the continuous phase above -1. The higher the value of this parameter, the lower the dissolution rate that is determined by the difference of the order parameters in the dispersed and the continuous phases. An increase in the dispersed phase volume fraction causes a faster increase in the order parameter that in its turn lowers the dissolution rate. The number concentration as a function of time is shown in Figure 9a. The change in time of

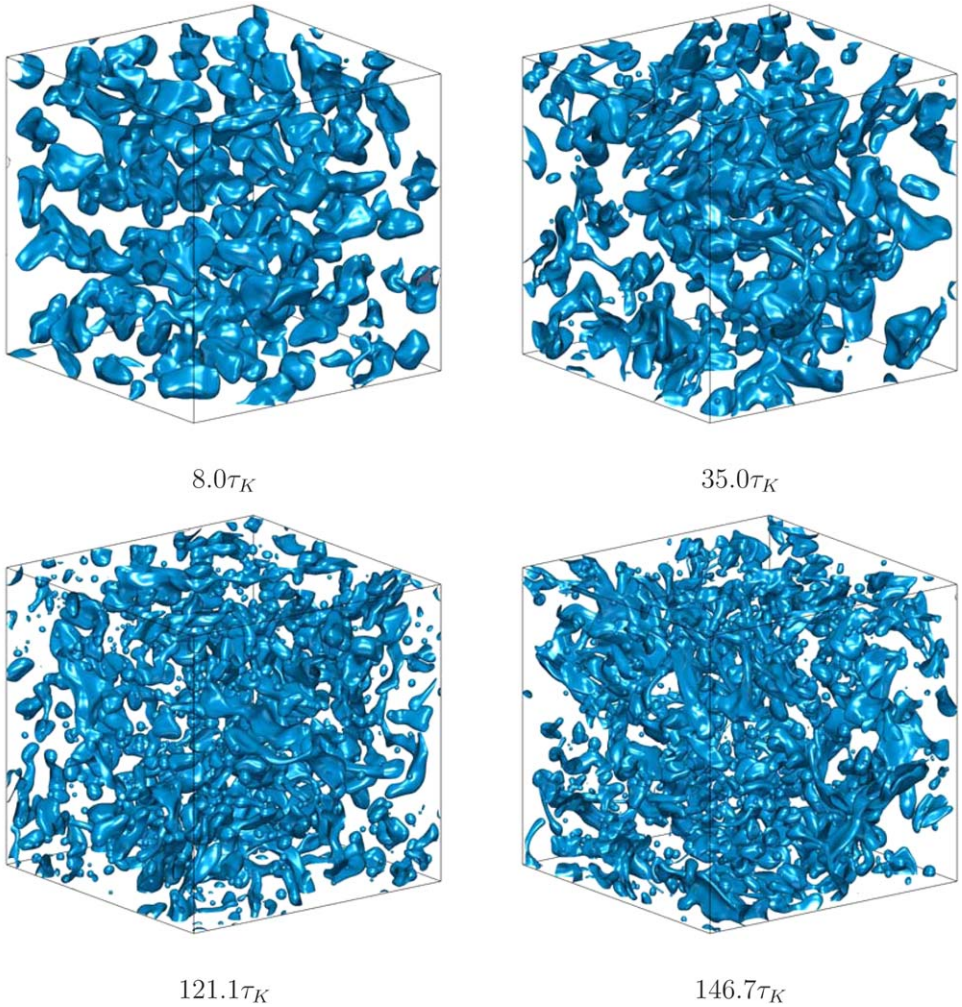

Figure 12. Isosurfaces of order parameter $\varphi = 0$ at different time instants relative to the Kolmogorov time scale τ_K for the case with $\eta_K = 2.5$ [lu] in a 1000^3 simulation domain; dispersed phase volume fraction is $\phi = 0.14$.

Viscosity ratio is $\lambda = 1$, capillary number $Ca = 0.004$. The moment of drop injection is $t = 0$. [Color figure can be viewed in the online issue, which is available at wileyonlinelibrary.com.]

dispersed phase volume relative to the initial value is depicted in Figure 9b. It can be seen from Figure 9b that for the dispersed phase volume fraction $\phi = 0.2$ the dissolution effect is effectively suppressed after a relatively short computation time and the V/V_{init} levels off to the value of 0.96. The simulation in this case runs long enough to reach a quasisteady state.

The isosurfaces of $\varphi = 0$ at different time instants for the cases of $\phi = 0.05$ and 0.2 are shown in Figure 10. The maximum drop diameter and the Sauter mean diameter are presented in Figures 11a and b, respectively. When $\phi = 0.2$, the $d_{\max}$ and d_{32} fluctuate around their average values.

The evolution of the dispersed phase in time for the simulation on the largest scale is shown in Figure 12. The dominant mechanism of drop breakup is end-pinching. At the early stage of the simulation, the number of drops reduced due to coalescence (e.g., at time instant $t = 35\tau_K$ there are 99 drops and there were 125 drops initially). Then complex drop deformations resulted in formation of numerous thin elongated structures. These structures are easily broken by turbulent eddies producing small drops as can be seen at time instants $121.1\tau_K$ and $146.7\tau_K$. For the simulated period of time, the maximum number of drops is 679 which is sufficient to estimate the statistics of the DSD.

It was shown experimentally, for instance, by Lovick et al.[55] and Pacek et al.[56] that the DSD of a liquid-liquid dispersion formed under turbulent flow conditions is close to a log-normal distribution. The DSD for the case with $\eta_K = 2.5$ [lu] and capillary number $Ca = 0.004$ is shown in Figure 13a at time instant $t = 117.9\tau_K$. Probability plots are used to assess whether data represent a certain distribution. In Figure 13b, the numerically obtained distribution is compared to a log-normal distribution. The midpoint probability plotting positions[57] are used. The ith sorted drop diameter value from a DSD of $N = 679$ drops is plotted against the midpoint in the jump of the log-normal cumulative distribution function on the y axis. The midpoint is calculated as $(i-0.5)/N$. The y axis scale is based on the log-normal distribution. As one can see from Figure 13b, the numerical data follow the distribution except for the smallest and largest droplets. Due to numerical dissolution, the overall number of drops is underestimated. At the same time, the number of small drops is overestimated, since drops dissolve every time step. The dynamic equilibrium between breakup and coalescence has

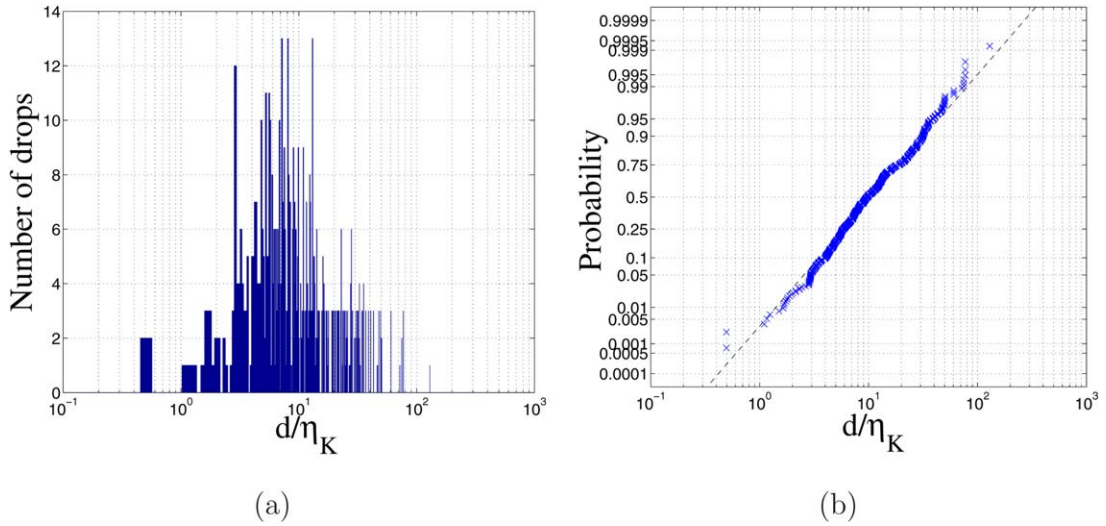

Figure 13. DSD (a) and log-normal probability plot (b) for the case with the Kolmogorov length scale resolution $\eta_K = 2.5$ [lu], viscosity ratio $\lambda = 1$, dispersed phase volume fraction $\phi = 0.14$, capillary number $Ca = 0.004$ at the time instant $t = 117.9\tau_K$.

There are 679 drops in the system. [Color figure can be viewed in the online issue, which is available at wileyonlinelibrary.com.]

not been reached yet for this simulation. Therefore, large droplets can break producing smaller fragments.

For the considered values of dispersed phase holdup it is not possible to obtain a dispersion: droplets continuously break and coalesce, and a large volume of dispersed phase remains connected (especially at $\phi = 0.2$). Even though the drops are broken into smaller drops, easy coalescence prevents dispersion formation. In diffuse interface methods, the drop interfaces have a finite thickness. If they overlap for sufficient time, the drops coalesce.[32] A possible way to suppress easy coalescence is a significant increase of resolution.[58] However, resolution requirements would be such that simulations of turbulent flow with multiple droplets involved will be computationally unaffordable. The overestimated coalescence rate is not the only reason that prevents dispersion formation. In practice, it is not always possible to disperse one immiscible liquid into another. For instance, Rueger and Calabrese[11] pointed out that it was not possible to achieve complete dispersion experimentally for certain pure systems above dispersed phase volume fraction 0.05. Only an addition of a sufficient amount of surfactant allowed to set stable dispersions up to $\phi = 0.5$.

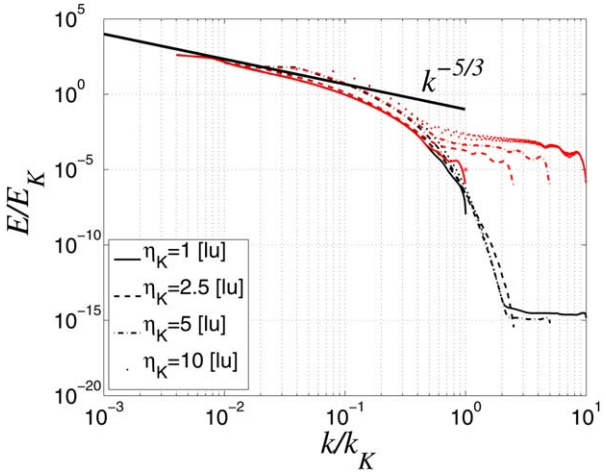

Figure 14. Kinetic energy spectrum in one- (black curves) and two-phase (red curves) systems for different resolution of Kolmogorov scales.

Energy is scaled with $E_K = \varepsilon^{2/3}\eta_K^{5/3}$; wave number is scaled with $k_K = 2\pi/\eta_K$. Marker * stands for the wavenumber corresponding to the Kolmogorov length scale η_K. Simulation domain edge $L_d = 500$ [lu]. [Color figure can be viewed in the online issue, which is available at wileyonlinelibrary.com.]

Energy spectra in one- and two-phase turbulent flow

The scale separation defined as ratio between the simulation domain edge length and the Kolmogorov length scale L_d/η_K indicates the possibility of developing an inertial energy subrange. Figure 14 shows the kinetic energy spectra of one-phase fully developed turbulent flow (black curves) for different cases of Kolmogorov scales resolution. The viscous subrange of the turbulent energy spectrum is always reproduced. The reproduction of the inertial subrange improves with the increase of L_d/η_K, and follows the slope of Kolmogorov universal scaling law ($E(k) \sim k^{-5/3}$) at small wavenumbers (or large length scales). The energy spectrum curve becomes horizontal at high wavenumbers k for $\eta_K = 5$ and 10 [lu] because at these values of k the machine accuracy is reached for the corresponding energy values E.

The kinetic energy spectrum changes dramatically when the second phase is injected. Energy spectra of one- and two-phase turbulent flows that correspond to different resolution of Kolmogorov scales are presented in Figure 14. As one can see, there is a significant energy gain at high wavenumbers or length scales which are of the order of and smaller than the Kolmogorov length scale η_K. This energy gain has a numerical background. Artificial numerical issues arise when velocities approach the magnitudes of spurious currents representing a numerical peculiarity of diffuse interface methods including LBE.[48] In two-phase turbulent flow, the velocity magnitude becomes comparable to the magnitude of spurious currents over the liquid-liquid interface. It is demonstrated in Figure 15 for the case of $\eta_K = 5$ and $\phi = 0.2$ that small amplitude velocity spikes appear on the

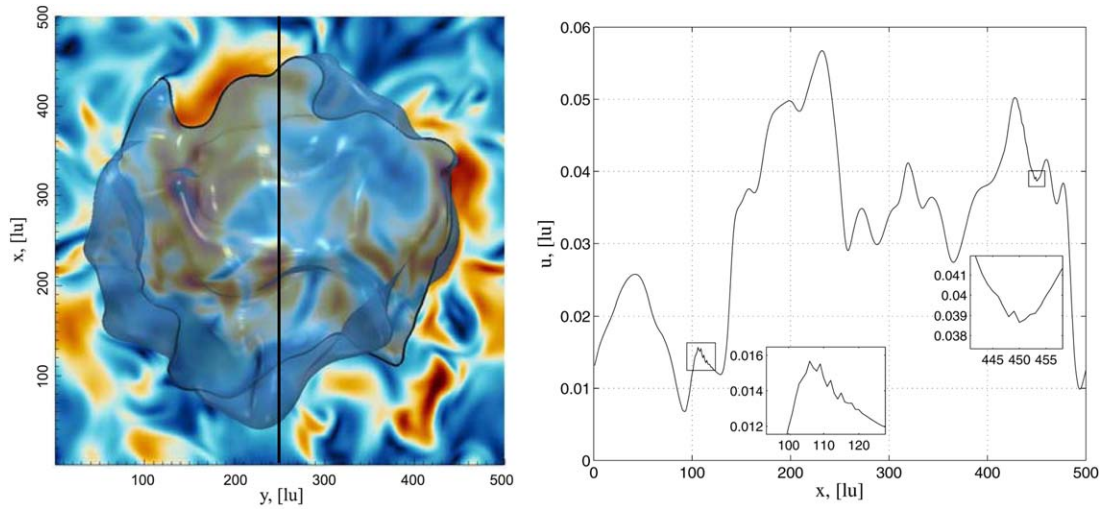

Figure 15. Deformed drop and velocity magnitude field (a); velocity magnitude along the black vertical line shown on the left (b).

The figure demonstrates the appearance of small velocity spikes over the liquid/liquid interface. [Color figure can be viewed in the online issue, which is available at wileyonlinelibrary.com.]

interfaces over the length scales in the range 1 to 10 lattice units which is smaller than and of the order of the Kolmogorov length scale. These spikes provide significant energy input in the viscous subrange. Furthermore, the energy gain is more notable for higher η_K resolution. Higher resolution of η_K means better representation of viscous energy subrange where small scale phenomena become more pronounced.

In every simulation performed, the maximum and the Sauter mean diameters are larger than the corresponding η_K. This means that drop sizes mainly fall in the inertial subrange of the energy cascade, and, therefore, we expect that the breakup and coalescence dynamics is not noticeably affected by the energy spikes appearing on scales that are smaller than η_K.

Conclusions

Numerical simulations of liquid-liquid dispersion formation in turbulent flow have been presented. A free energy lattice Boltzmann method was used to perform large-scale three-dimensional simulations of the binary system. Simulations were carried out in cubic fully periodic domains of 100^3 to 1000^3 lattice units. Homogeneous isotropic turbulence was generated throughout the domain by means of linear forcing. Liquids of equal density were considered. The viscosity ratio (dispersed phase over continuous phase viscosity) varied between $\lambda = 1$ and 0.3.

In each simulation, the process of dispersion formation is visualized. The number of drops in the system, the maximum drop diameter, and the Sauter mean diameter are all tracked as functions of time. An advantageous characteristic of the simulations compared to experiments is that the size of each drop can be measured in-line with no disturbance of the flow even for the dense dispersions. High resolution simulations of dispersion formation on the microscopic level allow observing the details of drop breakup and coalescence caused by interactions with turbulent eddies. It was outlined that in turbulent flow drops are mainly broken by end-pinching mechanism when bulbs form at the ends of the stretched drop and eventually pinch off. Thin threads can also form as a result of significant drop elongation before breakup. The threads break into small fragments either by capillary wave breakup or again by end-pinching. In addition, with the adopted mechanism of turbulence generation, the energy dissipation rate is used as an input parameter. Therefore, it is possible to correlate energy input and the resultant DSD of the dispersion.

However, several numerical issues are encountered. The method is plagued by numerical dissolution of small drops. It is demonstrated that in order to mitigate the drop dissolution effect, it is necessary to increase the resolution. Dissolution rate also decreases with the decrease of energy input and the increase of the concentration of the dispersed phase.

With the dispersed phase volume fraction higher than 0.05 and starting from a single drop it is not possible to form a dispersion, a large portion of dispersed phase remains connected. With an increase of the dispersed phase fraction, drop interactions become more frequent and most of them result in coalescence. Small droplets are more likely to coalesce rather than dissolve. In physical system, drops collide, form a thin film of continuous phase between them, the film drains, and eventually ruptures. Drops should be in contact sufficiently long for the film to drain and rupture. Otherwise, the collision is not efficient, and the drops do not merge. In numerical simulations of turbulent dispersion, the drop collision results in merging, except for several cases when the collision process is affected by interactions with turbulent eddies. Easy coalescence occurs because multiple drop interfaces can occupy the same computational cell. Thus, in order to suppress unphysical coalescence, it is necessary to resolve the film between the drops which requires enormous mesh resolution (see e.g., Ref. 58).

With the present implementation of the free energy LBE method, it is not possible to obtain a representative energy spectrum of two-phase turbulent flow. It is known that LBE methods are prone to generation of spurious currents due to

discretization of the velocity space. The order of magnitude of the velocity field can be comparable to the magnitude of the spurious currents. In addition, the spurious currents appear on the diffuse interface. They interfere with the Kolmogorov length scales that leads to a significant unphysical energy gain at high wavenumbers. The size of the resolved drops, the maximum drop diameter and the Sauter mean diameter, are larger than the corresponding η_K. Therefore, the breakup and coalescence dynamics is not affected by the energy spikes appearing on the scales, which are smaller and of the order of η_K.

Investigation of turbulent liquid-liquid systems is a challenging task for both experimental and numerical studies. Due to complexity of the system, there is no unequivocal choice on numerical method to handle these systems. This study demonstrates the capabilities and limitations of the free energy LBE method when performing DNSs of a liquid-liquid turbulent flow and creates the basis for further investigations. Therefore, it is shown what to expect from the method and how to assess the results.

Three drawbacks were outlined. First, the numerical dissolution of small drops. This effect is unavoidable in the context of Cahn-Hilliard dynamics. However, there are ways to mitigate drop dissolution, for instance, to increase the resolution (increase the minimum size of the drops), or choose different formulation of the free energy functional.[31] It is important to keep in mind that it is also difficult to track small drops experimentally: they can (physically) dissolve, or when estimating the DSD, the drops can be too small to be captured.

Second drawback is over-estimation of drop coalescence rate. At the present time, handling coalescence is not straightforward in any numerical method dealing with three-dimensional simulations: if no special treatments are performed (e.g., addition of surfactant to physically suppress drop coalescence) drops either coalescence easily or they do not, and artificial "cut-and-connect" algorithms are required to merge them.

Finally, the appearance of spurious currents leading to energy gain at high wavenumbers is observed. This issue is not specific to free energy LBE approach (see e.g., Ref. 59 discussing spurious currents in VOF methods). If physical velocities are an order of magnitude larger than spurious velocities, the spurious currents effect can be mitigated to some extent.

Despite these drawbacks, the results are encouraging. The DSD of the large scale simulation that takes into account microscopic drop-drop and drop-eddy interactions reflects the experimental observations and follows the log-normal distribution. Having numerical dissolution of small drop and easy-coalescence in mind, it is possible to investigate the relative effect of the energy input on the DSD. Additionally, the sensitivity of the DSD with respect to viscosity ratio and interfacial tension between the liquids can also be addressed. When the drawbacks of the method are minimized or resolved, the developed approach could be used to broaden the understanding of liquid-liquid dispersion process. As dispersed and continuous phase interactions in well-controlled homogeneous isotropic turbulent flow are resolved on microscopic level, it is possible to derive more fundamental breakup and coalescence kernels even for dense systems which can be used in population balance equations or multiscale simulations in future.

Literature Cited

1. Pope SB. Turbulent flows. Cambridge; New York: Cambridge University Press, 2000.
2. Berkman PD, Calabrese RV. Dispersion of viscous liquids by turbulent flow in a static mixer. *AIChE J*. 1988;34:602–609.
3. Brown DE, Pitt K. Drop size distribution of stirred non-coalescing liquid-liquid system. *Chem Eng Sci*. 1972;27:577–583.
4. Calabrese RV, Chang TPK, Dang PT. Drop breakup in turbulent stirred-tank contactors. Part I: effect of dispersed-phase viscosity. *AIChE J*. 1986;32:657–666.
5. Collins SB, Knudsen JG. Drop-size distributions produced by turbulent pipe flow of immiscible liquids. *AIChE J*. 1970;16:1072–1080.
6. Davies JT. A physical interpretation of drop sizes in homogenizers and agitated tanks, including the dispersion of viscous oils. *Chem Eng Sci*. 1987;42:1671–1676.
7. Sleicher CA. Maximum stable drop size in turbulent flow. *AIChE J*. 1962;8:471–477.
8. Weinstein B, Treybal RE. Liquid-liquid contacting in unbaffled, agitated vessels. *AIChE J*. 1973;19:304–312.
9. Paul EL, Atiemo-Obeng VA, Kresta CM, editors. Handbook of Industrial Mixing: Science and Practice. Hoboken, New Jersey: Wiley, 2004.
10. Boxall JA, Koh CA, Sloan ED, Sum AK, Wu DT. Droplet size scaling of water-in-oil emulsions under turbulent flow. *Langmuir*. 2011; 28:104–110.
11. Rueger PE, Calabrese RV. Dispersion of water into oil in a rotor-stator mixer. Part 1: Drop breakup in dilute systems. *Chem Eng Res Des*. 2013;91:2122–2133.
12. Rueger PE, Calabrese RV. Dispersion of water into oil in a rotor-stator mixer. Part 2: Effects of phase fraction. *Chem Eng Res Des*. 2013;91:2134–2141.
13. Rallison JM, Acrivos A. A numerical study of the deformation and burst of a viscous drop in an extensional flow. *J Fluid Mech*. 1978; 89:191–200.
14. Unverdi S, Tryggvason G. A front-tracking method for viscous, incompressible, multi-fluid flows. *J Comput Phys*. 1992;100:25–37.
15. Peskin CS. Flow patterns around heart valves: a digital computer method for solving the equations of motion. PhD thesis, Physiology, Albert Einstein College of Medicine, University Microfilms, 378:72–30, 1972.
16. Osher S, Sethian J. Fronts propagating with curvature-dependent speed: algorithms based on Hamilton–Jacobi formulations. *J Comput Phys*. 1988;79:12–49.
17. Lafaurie B, Nardone C, Scardovelli R, Zaleski S, Zanetti G. Modelling merging and fragmentation in multiphase flows with SURFER. *J Comput Phys*. 1978;113:134–147.
18. Sussman M, Puckett EG. A coupled level set and volume-of-fluid method for computing 3D and axisymmetric incompressible two-phase flows. *J Comput Phys*. 2000;162:301–337.
19. Cristini V, Tan YC. Theory and numerical simulation of droplet dynamics in complex flows—a review. *Lab Chip*. 2004;4:257–264.
20. Swift MR, Orlandini E, Osborn WR, Yeomans JM. Lattice Boltzmann simulations of liquid-gas and binary fluid systems. *Phys Rev E*. 1996;54:5041–5052.
21. Peng Y, Liao W, Luo LS, Wang LP. Comparison of the lattice Boltzmann and pseudo-spectral methods for decaying turbulence: low-order statistics. *Comput Fluids*. 2010;39:568–591.
22. Derksen JJ, Van den Akker HEA. Multi-scale simulations of stirred liquid-liquid dispersions. *IChemE*. 2007;85:697–702.
23. He X, Chen S, Zhang R. A lattice Boltzmann scheme for incompressible multiphase flow and its aplication in smulation of Rayleigh-Taylor instability. *J Comput Phys*. 1999;152:642–663.
24. Toschi F, Perlekar P, Biferale L, Sbragaglia M. Droplet breakup in homogeneous and isotropic turbulence. arXiv:1010.1795, pages 1–4, 2010.
25. Shan X, Chen H. Lattice Boltzmann model for simulating flows with multiple phases and components. *Phys Rev E*. 1993;47:1815–1819.
26. Biferale L, Perlekar P, Sbragaglia M, Srivastava S, Toschi F. A lattice Boltzmann method for turbulent emulsions. *J Phys Conf Ser*, 2011;318:052017.
27. Skartlien R, Sollum E, Schumann H. Droplet size distributions in turbulent emulsions: breakup criteria and surfactant effects from direct numerical simulations. *J Chem Phys*. 2013;139:174901.
28. Nekovee M, Coveney PV, Chen H, Boghosian BM. Lattice-Boltzmann model for interacting amphiphilic fluids. *Phys Rev E*. 2000;62:8282–8294.
29. Baraldi A, Dodd MS, Ferrante A. A mass-conserving volume-of-fluid method: volume tracking and droplet surface-tension in incompressible isotropic turbulence. *Comput Fluids*. 2014;96:322–337.

30. Lundgren TS. Linearly forced isotropic turbulence. *Annu Res Briefs*. 2003:461–473.
31. Keestra BJ, Van Puyvelde PCJ, Anderson PD, Meijer HEH. Diffuse interface modeling of the morphology and rheology of immiscible polymer blends. *Phys Fluids*. 2003;15:2567–2575.
32. Jia X, McLaughlin JB, Kontomaris K. Lattice Boltzmann simulations of flows with fluid–fluid interfaces. *Asia-Pac J Chem Eng*. 2008;3: 124–143.
33. Komrakova AE, Shardt O, Eskin D, Derksen JJ. Lattice Boltzmann simulations of drop deformation and breakup in shear flow. *Int J Multiphase Flow*. 2014;126:24–43.
34. Komrakova AE, Shardt O, Eskin D, Derksen JJ. Effects of dispersed phase viscosity on drop deformation and breakup in inertial shear flow. *Chem Eng Sci*. 2015;126:150–159.
35. Cutter LA. Flow and turbulence in a stirred tank. *AIChE J*. 1966;12: 35–45.
36. Zhou G, Kresta SM. Correlation of mean drop size and minimum drop size with the turbulence energy dissipation and the flow in an agitated tank. *Chem Eng Sci*. 1998;53:2063–2079.
37. Hinze JO. Fundamentals of the hydrodynamic mechanism of splitting in dispersion processes. *AIChE J*. 1955;1:289–295.
38. Jacqmin D. Calculation of two-phase Navier–Stokes flows using phase–field modeling. *J Comput Phys*. 1999;155:96–127.
39. Magaletti F, Picano F, Chinappi M, Marino L, Casciola CM. The sharp-interface limit of the Cahn-Hilliard/Navier-Stokes model for binary fluids. *J Fluid Mech*. 2013;714:95–126.
40. Yue P, Feng JJ, Liu C, Shen J. A diffuse-interface method for simulating two-phase flows of complex fluids. *J Fluid Mech*. 2004;515: 293–317.
41. Badalassi VE, Ceniceros HD, Banerjee S. Computation of multiphase systems with phase field models. *J Comp Phys*. 2003;190: 371–397.
42. Cahn JW, Hilliard JE. Free energy of a nonuniform system. I. Interfacial free energy. *J Chem Phys*. 1958;28:258–267.
43. Penrose O, Fife P. Thermodynamically consistent models of phase-field type for the kinetics of phase transitions. *Phys D*. 1990;43:44–62.
44. Bray AJ. Theory of phase-ordering kinetics. *Adv Phys*. 1994;43:357–459.
45. Kendon VM, Cates ME, Pagonabarraga I, Desplat JC, Bladon P. Inertial effects in three–dimensional spinodal decomposition of a symmetric binary fluid mixture: a lattice boltzmann study. *J Fluid Mech*. 2001;440:147–203.
46. Bhatnagar PL, Gross EP, Krook M. A model for collision processes in gases. I. Small amplitude processes in charged and neutral one-component systems. *Phys Rev*. 1954;94:511–525.
47. Kusumaatmaja H. Lattice Boltzmann studies of wetting and spreading on patterned surfaces. PhD thesis, England: University of Oxford, 2008.
48. Van der Sman RGM, Van der Graaf S. Emulsion droplet deformation and breakup with lattice Boltzmann model. *Comp Phys Commun*. 2008;178:492–504.
49. Rosales C, Meneveau C. Linear forcing in numerical simulations of isotropic turbulence: physical space implementations and convergence properties. *Phys Fluids*. 2005;17:095106.
50. Derksen JJ. Flow-induced forces in sphere doublets. *J Fluid Mech*. 2008;608:337–356.
51. Valino L, Martin J, Hazi G. Dynamics of isotropic homogeneous turbulence with linear forcing using a lattice Boltzmann method. *Flow Turbulence Combust*. 2010;84:219–237.
52. Sankaranarayanan K, Kevrekidis IG, Sundaresan S, Lu J, Tryggvason G. A comparative study of lattice Boltzmann and front-tracking finite-difference methods for bubble simulations. *Int J Multiphase Flow*. 2003;29:109–116.
53. Marks C. Drop breakup and deformation in sudden onset strong flows. PhD thesis, USA: University of Maryland, 1998.
54. Khismatullin DB, Renardy Y, Cristini V. Inertia-induced breakup of highly viscous drops subjected to simple shear. *Phys Fluids*. 2003; 15:1351–1354.
55. Lovick J, Mouza AA, Paras SV, Lye GJ, Angeli P. Drop size distribution in highly concentrated liquid–liquid dispersions using a light back scattering method. *J Chem Technol Biotechnol*. 2005;80:545–552.
56. Pacek AW, Man CC, Nienow AW. On the Sauter mean diameter and size distributions in turbulent liquid/liquid dispersions in a stirred vessel. *Chem Eng Sci*. 1998;53:2005–2011.
57. MATLAB and Statistics Toolbox Release 2014b. The MathWorks, Inc., Natick, Massachusetts.
58. Shardt O, Derksen JJ, Mitra SK. Simulations of droplet coalescence in simple shear flow. *Langmuir*. 2013;29:6201–6212.
59. Renardy Y, Renardy M. PROST: a parabolic reconstruction of surface tension for the volume-of-fluid method. *J Comput Phys*. 2002; 183:400–421.

Manuscript received Aug. 25, 2014, and revision received Dec. 2, 2014.